Magnetic susceptibility measurement and modelisation of a novel compound.

by

Bastien Dalla Piazza

Supervisor : Pr. Henrik Ronnow
Co-supervisor : Gøran Nilsen

January 13, 2008

Abstract

We study the magnetic susceptibility of the novel metal-organic framework $\{[Cu_3(\mu_3 - O)(\mu_3 - trz)_3(OH)(H_2O)_6]\}_n$. The magnetic susceptibility is measured using a SQUID magnetometer. Exact diagonnalization and mean field theory are then used in an attempt to fit the experimental data.

Contents

1 Introduction.

Geometrically frustrated systems have given rise to a strong interest since almost two decades starting with the study of the spin glasses. Such systems shows a great deal of interesting behaviours such as a highly degenerate ground state, a suppression of the magnetic ordering and unconventional spin states like spin liquids. Both exact or effective models have been developed and can be investigated through experiments [1][2][3] . In this context, synthesis and analysis of novel frustrated compounds can bring new information. Numerical approaches have proven to be really efficient in many domains. But frustrated systems are really numerically challenging. Quantum Monte Carlo simulation, one of the most powerfull tool offered by the numerical approach, fails for such systems because of the so-called sign problem. One is often left with only exact diagonnalization as a numercial tool. But full diagonnalization algorythms are of cubic complexity in the size of the matrix which limits dramatically the size of the matrices one want to diagonnalize in a reasonnable time, not to mention the memory usage limits due to the storage of huge dense matrices. The numerical approach we used in this project had to deal with all these limitations.
The metal-organic framework $\{[Cu_3(\mu_3 - O)(\mu_3 - trz)_3(OH)(H_2O)_6]\}_n$ [4] is typically geometrically frustrated. Although experimentally measuring the susceptibility of materials is not of a great difficulty, fitting it to one of the effective model is not a simple task. Indeed, the complexity of such models increase dramatically with the size of the system. It is therefore mandatory to use numerical analysis to get the susceptibility curves. Most of the work done in this research project is about performing these numerical computations in order to reproduce the features found in the experimental data and fit it if possible.

2 Chemical and crystallographic characterisation.

Synthesis and analysis of the metal-organic framework $\{[Cu_3(\mu_3-O)(\mu_3-trz)_3(OH)(H_2O)_6]\}_n$ (Cutrz) has been done by Ding, B. *et al.* [4]. It has been synthesised by heating a mixture of triazole, $CuSO_4 \cdot 5H_2O$ and aqueous ammonia. In this solution, the Cu ions with the triazole form the trimers $Cu_3(\mu_3 - O)$. While cooling down, the metal-organic framework precipitates and one can isolate it from the ammonia solution. The Cutrz is then a blue powder of small cubic crystals.
For this study, the compound itself has been provided by the Solid State Chemistry group of Karl Krämer at the Department of Chemistry and Biochemistry in Bern, Switzerland. The powder X-ray diffraction analysis shows that Cutrz is made of trinuclear triangular Cu^{II} secondary building units bounded together by triazolatos. Four of these trimers form a molecular cage that can be interpreted as a tertiary building unit (fig. 2.2). The whole structure is cubic. The distance between the Cu's within a trimer is 3.388 Å and the shortest distance between the trimers is 6.022 Å. The complete cell is shown in fig. 2.1 in the [001] direction. The magnetic characteristics rely only on the Cu^{II}'s. Each Cu^{II} carries a single spin degree of freedom. There are two magnetic couplings that obviously need to be taken in account. The first is the coupling inside the trimer, i. e. the intra-trimer coupling. The second one is the coupling between the trimers, i. e. the inter-trimer coupling. These two couplings correspond to the two distances defined before (the intra-trimer distance between the Cu^{II} and the shortest inter-trimer distance) and are shown as bonds in fig.2.3.

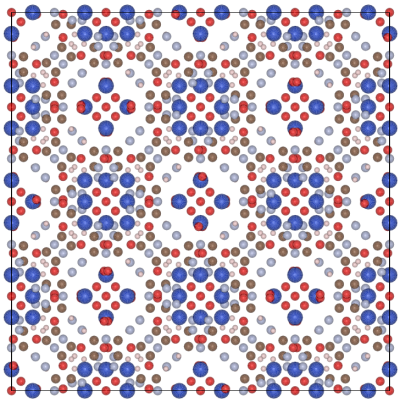

Figure 2.1: The whole Cutrz cell viewed in the [001] direction (Blue: Cu, red: O, braun: C, light blue: N, light pink: H).

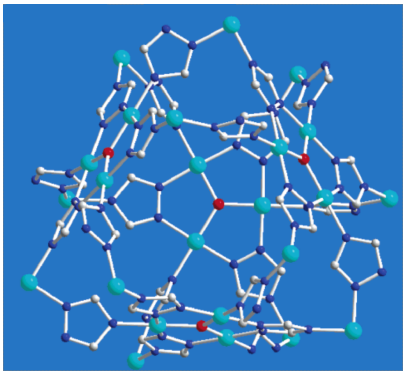

Figure 2.2: Molecular cage. Four trimers oriented in the four different planes defines this molecular cage. The image is from the paper of Ding, B *et al.* [4].

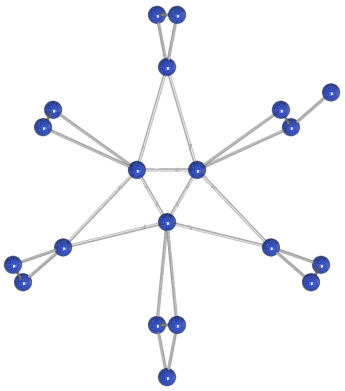

Figure 2.3: A plane of interacting trimers in the [111] direction.

3 SQUID susceptibility measurements.

3.1 SQUID magnetometer.

We briefly describe the Superconducting Quantum Interference Device (SQUID). The squid central component is two or more superconducting elements coupled by Josephson junctions [5] forming a loop (fig. 3.1). Since there is no scattering in the superconducting elements, the current is only limited by the very tiny i_c of the Josephson junctions. The current being very small, the electron pair wave function has a very long wave length. In the absence of an external field, the phase difference between two points in the loop is almost null. A phase difference is therefore only due to external field.

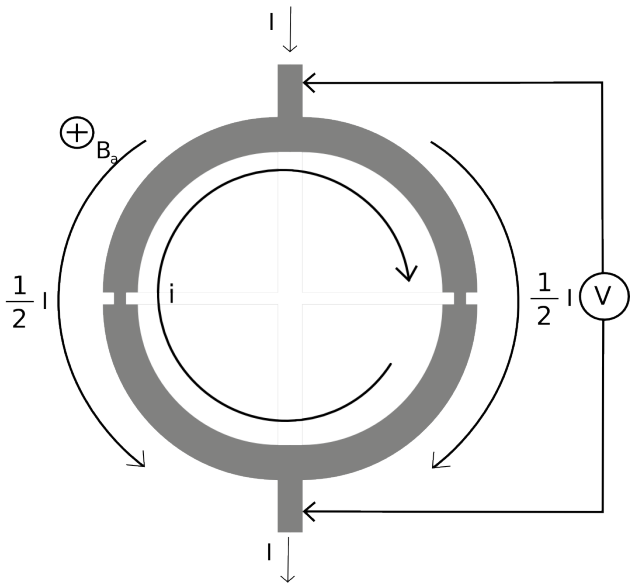

Figure 3.1: SQUID supraconducting loop.

On the whole loop, the phase difference must be a integer multiple of 2π. If there is an applied field B causing a phase difference $\Delta\phi(x)$, a current i will appear to meet the condition:

$$\Delta\phi(x) + 2\Delta\phi(i) = n \cdot 2\pi. \tag{3.1}$$

The current i is what one need to measure to determine the applied field B. In order to measure it, a measuring current I is applied (fig. 3.1). If the current is small, no voltage will be detected because of the superconducting elements. But from a critical current I_c, the Josephson junctions will cause a voltage to be measured. This critical current is what is being measured. The relation between the applied field ϕ_a and the critical current I_c is:

$$I_c = 2i_c \left| cos\left(\pi \frac{\phi_a}{\phi_0}\right)\right| \tag{3.2}$$

Where i_c is the critical current through the Josephson junction and ϕ_0 is a quantised quantity called a fluxon:

$$\phi_0 = \frac{h}{2e} = 2.07 \times 10^{-15} \quad Wb. \tag{3.3}$$

The current I_c is oscillating as the ratio $\frac{\phi_a}{\phi_0}$. Measuring these oscillations allows to see changes in the magnetic field of the order of ϕ_0.

3.2 Measurements.

The susceptibility is defined as:

$$\chi_M = \frac{\partial M}{\partial H} \tag{3.4}$$

where M is the magnetisation and H is the applied field. To measure a compound's susceptibility, one introduce it in a straw. The straw goes slowly in several steps through the superconducting ring while an external field is applied. While going through the superconducting ring, the response of the compound to the applied field will cause the measured field to change, hence the susceptibility is measured. Usually, the

magnetisation is very accurately linear in H for attainable field strength, so the susceptibility measurement does not depend on the intensity of the applied field.
The results of the measurements are shown in fig. 3.2 and 3.3. Two measurements were performed with two different samples. The first one motivated this study (green line) and the second one (blue line) was obtained later. The shift between the two measurements is due to a diamagnetic background probably due to oxides. The second sample appear purer than the first one.

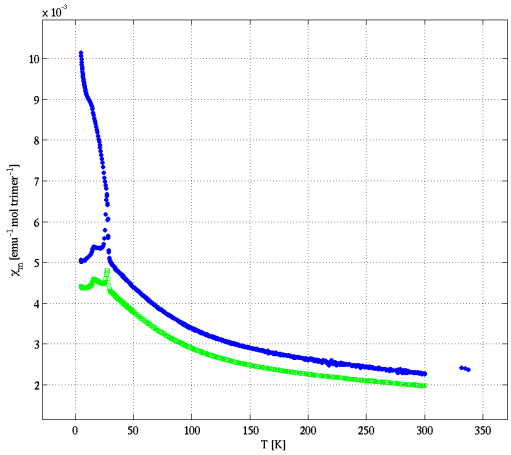

Figure 3.2: Susceptibility measurement of the metal-organic framework $\{[Cu_3(\mu_3 - O)(\mu_3 - trz)_3(OH)(H_2O)_6]\}_n$.

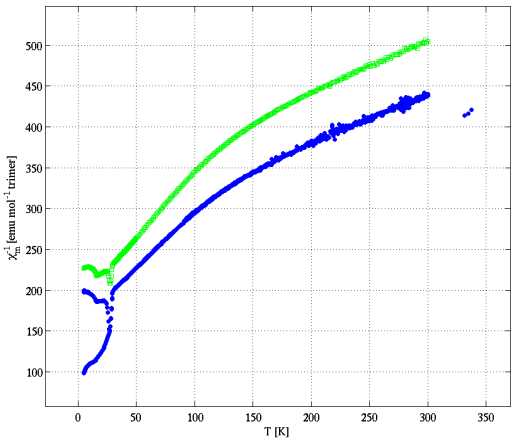

Figure 3.3: Inverse susceptibility measurement of the metal-organic framework $\{[Cu_3(\mu_3 - O)(\mu_3 - trz)_3(OH)(H_2O)_6]\}_n$.

Fig. 3.2 shows at least one phase transition around $15K$. We did not study the nature of the phase transitions since our study intends to fit the data at higher temperatures without magnetic ordering, although the phase transition around $15K$ could be for example a Neel ordered phase. The high temperature part ($T > 50K$) of fig. 3.3 is what is actually studied. One can see two slopes in the inverse susceptibility (χ^{-1}) characteristic of the trimer susceptibility. But the second slope (the sharpest) does not go to zero (infinite susceptibility) as does the trimer one. This is due to inter-trimer magnetic couplings. This inter-trimer coupling effect is studied section 4 and 5.

4 Modelising.

The purpose of this study is to model the magnetic behaviour of the Cutrz at high T. As explained in section 2, the magnetic behaviour relies only on the Cu^{II}. In the crystal, the copper has lost two of his electrons, so there are nine electrons in the 3d electronic level, thus a spin-$\frac{1}{2}$ degree of freedom. Copper oxides are therefore ideal to study magnetism in condensed matter.
We model the magnetic cell by defining a site carrying a spin-$\frac{1}{2}$ for each copper found in the crystallographic data. Only two magnetic couplings are taken in account, the intra-trimer coupling J_1 and the inter-trimer coupling J_2. The physics is then described using the Heisenberg model:

$$H = -J_1 \sum_{\langle i,j \rangle} \vec{S_i} \cdot \vec{S_j} - J_2 \sum_{\langle\langle i,j \rangle\rangle} \vec{S_i} \cdot \vec{S_j} \tag{4.1}$$

Where $\langle i,j \rangle$ denotes the first neighbours (the intra-trimer coupling) and $\langle\langle i,j \rangle\rangle$ denotes the second neighbours (the inter-trimer coupling). The $\vec{S_i}$ are the usual spin-$\frac{1}{2}$ operators.

The product $\vec{S_i} \cdot \vec{S_j}$ can be rewritten as:

$$\vec{S_i} \cdot \vec{S_j} = S_i^z S_j^z + \frac{1}{2}(S_i^+ S_j^- + S_i^- S_j^+) \tag{4.2}$$

We can therefore construct the basis of states using the z projections of the spins. We now see that the Hamiltonian is split in two parts, a diagonal one and an off-diagonal one, the $S_i^+ S_j^-$ products being spin flips.
By definition, there are two states available for each site : $\{\uparrow, \downarrow\}$. The basis size is therefore:

$$card(\mathcal{H}) = 2^N \tag{4.3}$$

Where N is the number of sites. If one want to write the matrix representation of the Hamiltonian in this basis, the matrix size is 2^{2N}.
But the Hamiltonian 4.1 has another property. Since it is quadratic in the spin operators, one can conclued that the quantum number S_{total}^z is conserved, i. e. the sum of the z-component at each site. That means that the matrix representation of the Hamiltonian 4.1 is block-diagonal. Some simple combinatorics allows to find the cardinality of the S_{total}^z sub-sectors.
Let N be the number of sites, $n_\uparrow$ the number of spins up and $n_\downarrow$ the number of spins down. We have the following constraints:

$$n_\uparrow + n_\downarrow = N \tag{4.4}$$

$$\frac{1}{2}(n_\uparrow - n_\downarrow) = S_{total}^z \tag{4.5}$$

leading to:

$$n_\uparrow = \frac{1}{2}N + S_{total}^z \tag{4.6}$$

Starting with an empty lattice, the number of ways to place $n_\uparrow$ spins up is:

$$\frac{N(N-1)\dots(N-n_\uparrow)}{n_\uparrow!} \tag{4.7}$$

Where we have to divide by $n_\uparrow!$ to not take in account the permutations of the same spins. Similarly, the number of ways to place $n_\downarrow$ spins down after placing the $n_\uparrow$ spins up is:

$$\frac{(N-n_\uparrow-1)(N-n_\uparrow-2)\dots 2\cdot 1}{n_\downarrow!} \tag{4.8}$$

The cardinality of the S_{total}^z sub-sectors is therefore:

$$card(\mathcal{H}_{n_\uparrow}) = \frac{N(N-1)\dots(N-n_\uparrow)(N-n_\uparrow-1)(N-n_\uparrow-2)\dots 2\cdot 1}{n_\uparrow!(N-n_\uparrow)!} \tag{4.9}$$

$$= \frac{N!}{n_\uparrow!(N-n\uparrow)!} \tag{4.10}$$

From the previous relation it is obvious that the bigger S_{total}^z sub-sector will be the one for $S_{total}^z = 0$.

4.1 Magnetic lattice.

The magnetic lattice is rather difficult to describe. The inter-trimer couplings should be the most important guideline to follow. As already shown on fig. 2.3, each given trimer interacts with six others within a plane. We show again the picture from fig. 4.1 for convenience.

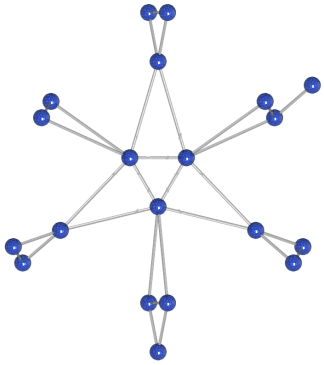

Figure 4.1: A plane of interacting trimers in the [111] direction.

If we look at the lattice along the [110], [101] or [011] direction, one can see lines of trimers pointing along these axes, but alternatively rotated around these axes by $\frac{\pi}{4}$ (fig. 4.2). Each of these trimers define the plane it is interacting in (fig. 4.3). One can see on fig. 4.3 how every consecutive planes are rotated by $\frac{\pi}{4}$.

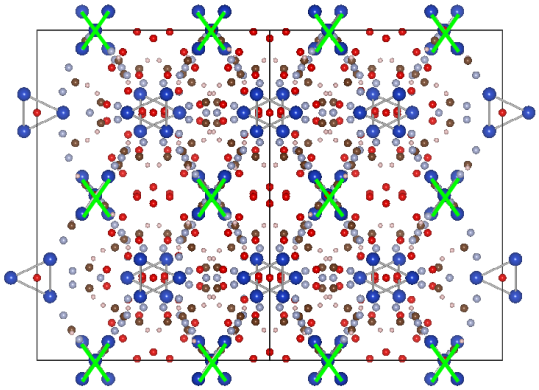

Figure 4.2: Cutrz crystal viewed along the [011] direction. The trimers are shown by the bonded Cu (blue). One can see aligned trimers along the [011] direction marked with the green crosses.

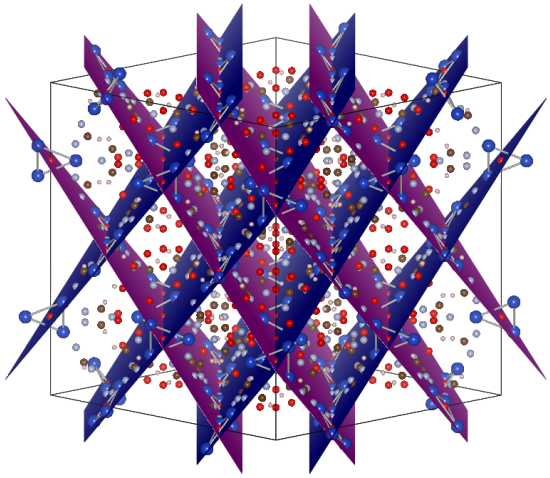

Figure 4.3: Alternatively rotated planes in whichone the aligned trimers (fig. 4.2) interacts with six other trimers.

There seems to be no obvious way to reduce this lattice to a simpler one. As a guideline for the further investigations, one can just retain the most important topological facts. The first one is the spins being parts of trimers. the second one is that each trimer is coupled to six other as shown in fig. 4.1.

4.2 Analytic approaches.

4.2.1 Exact trimer diagonnalization.

As a starting point, one can consider that the inter-trimer coupling J_2 will be significantly smaller than the intra-trimer coupling, and therefore be of negligible effect at high temperatures. The first thing to do is then to derive the magnetic susceptibility of a trimer.

The basis can be split in several parts according to the total spin since the Heisenberg Hamiltonian conserves the total spin:

$$S^z_{total} = \frac{3}{2} \qquad \mathcal{H}_{\frac{3}{2}} = \{(\uparrow\uparrow\uparrow)\} \tag{4.11}$$

$$S^z_{total} = \frac{1}{2} \qquad \mathcal{H}_{\frac{1}{2}} = \{(\uparrow\uparrow\downarrow), (\uparrow\downarrow\uparrow), (\downarrow\uparrow\uparrow)\} \tag{4.12}$$

$$S^z_{total} = -\frac{1}{2} \qquad \mathcal{H}_{-\frac{1}{2}} = \{(\uparrow\downarrow\downarrow), (\downarrow\uparrow\downarrow), (\downarrow\downarrow\uparrow)\} \tag{4.13}$$

$$S^z_{total} = -\frac{3}{2} \qquad \mathcal{H}_{-\frac{3}{2}} = \{(\downarrow\downarrow\downarrow)\} \tag{4.14}$$

We recall that the Hamiltonian is:

$$H = -J_1 \sum_{\langle i,j \rangle} \vec{S_i} \cdot \vec{S_j} = -J_1 \sum_{\langle i,j \rangle} S^z_i S^z_j + \frac{1}{2}(S^+_i S^-_j + S^-_i S^+_j) \tag{4.15}$$

The biggest matrix one has to diagonalise is therefore just the 3 by 3 matrix found for $\mathcal{H}_{\frac{1}{2}}$ and $\mathcal{H}_{-\frac{1}{2}}$:

$$\hat{H} = \frac{1}{4}|J_1| \begin{pmatrix} -1 & 2 & 2 \\ 2 & -1 & 2 \\ 2 & 2 & -1 \end{pmatrix} \tag{4.16}$$

Where J_1 has been taken negative (antiferromagnetic). The following eigenvalues are found:

$$S^z_{total} = \frac{3}{2} \qquad \{\frac{3}{4}|J_1|\} \tag{4.17}$$

$$S^z_{total} = \frac{1}{2} \qquad \{\frac{3}{4}|J_1|, \frac{3}{4}|J_1|, -\frac{3}{4}|J_1|\} \tag{4.18}$$

$$S^z_{total} = -\frac{1}{2} \qquad \{\frac{3}{4}|J_1|, \frac{3}{4}|J_1|, -\frac{3}{4}|J_1|\} \tag{4.19}$$

$$S^z_{total} = -\frac{3}{2} \qquad \{\frac{3}{4}|J_1|\} \tag{4.20}$$

We find the molar magnetic susceptibility with:

$$\chi_M = \frac{N_A(\mu_B g)^2}{k_B T}\left(\langle m^2\rangle - \langle m\rangle^2\right) \tag{4.21}$$

Where μ_B is the Bohr magneton and g is the electronic g-factor (equal to 2.0023 in the hollow). The brackets denote the usual Boltzmann statistical average:

$$\langle A\rangle = \frac{\sum_i A exp(-\beta E_i)}{\sum_i exp(-\beta E_i)} \tag{4.22}$$

$\langle m\rangle$ is found to be null. For $\langle m^2\rangle$:

$$\langle m^2\rangle = \frac{5exp\left(-\frac{3}{4}|J_1|\beta\right) + exp\left(\frac{3}{4}|J_1|\beta\right)}{4\left(exp\left(-\frac{3}{4}|J_1|\beta\right) + exp\left(\frac{3}{4}|J_1|\beta\right)\right)} \tag{4.23}$$

$$= \frac{5exp\left(-\frac{3}{2}|J_1|\beta\right) + 1}{4\left(exp\left(-\frac{3}{2}|J_1|\beta\right) + 1\right)} \tag{4.24}$$

Bringing 4.21 and 4.24 together gives the exact analytical magnetic susceptibility for the the trimer:

$$\chi_M = \frac{N_A(\mu_B g)^2}{k_B T}\frac{5exp\left(-\frac{3}{2}|J_1|\beta\right) + 1}{4\left(exp\left(-\frac{3}{2}|J_1|\beta\right) + 1\right)} \tag{4.25}$$

We plot this expression in fig. 4.4 and the inverse susceptibility in fig. 4.5. The second plot is instructive if we compare it to the Curie-Weiss susceptibility:

$$\chi_M = \frac{C}{T-\theta} \tag{4.26}$$

We see that the two slopes found in fig. 4.5 corresponds to two Curie-Weiss regimes. A detailed discussion of this is carried out in section 5.

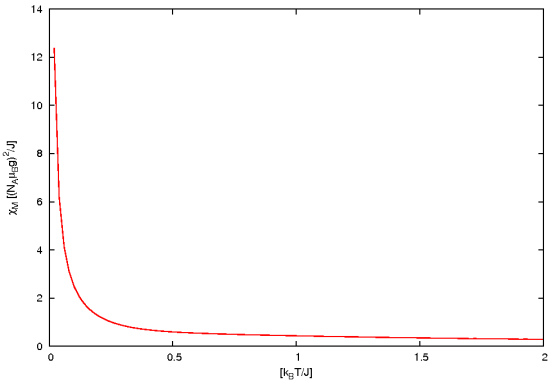

Figure 4.4: Temperature dependence of the exact magnetic susceptibility of the trimer.

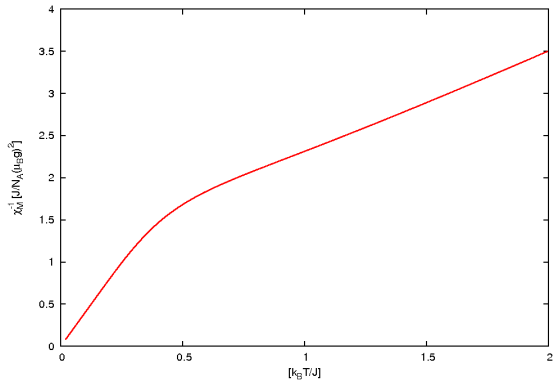

Figure 4.5: Inverse susceptibility temperature dependence of the trimer.

4.2.2 Mean field approach.

In a mean field approach, one can consider the interaction of trimers over a given trimer as an external magnetic field. The assumption here is that the different trimer states are uncorrelated which is of course wrong in the strongly interacting limit. Nonetheless the mean field approach often brings valuable information and is usually easy to apply. We model the effective magnetic field as follow:

$$\vec{H_{eff}} = \vec{H} + \lambda \vec{M} \tag{4.27}$$

Where

$$\lambda = \frac{N_A z J_2}{(g\mu_B)^2}, \quad z = 6 \quad \text{(trimer coordination number)} \tag{4.28}$$

Using that expression, one gets a consistency equation for the mean trimer magnetisation density:

$$M = M_0 \left(\frac{H_{eff}}{T} \right). \tag{4.29}$$

the overall magnetic susceptibility is then computed:

$$\chi = \left. \frac{\partial M}{\partial H} \right|_{H=0} = \left. \frac{\partial M_0}{\partial H} \left(\frac{H_{eff}}{T} \right) \right|_{H=0} + \frac{M_0}{T} \tag{4.30}$$

with the Curie law $\chi = \frac{M}{T}$:

$$\chi = \chi_0 \left(1 + \lambda \frac{M}{T} \right) = \chi_0 \left(1 + \lambda \chi \right) \tag{4.31}$$

leading to the solution:

$$\chi = \frac{\chi_0}{1 - \lambda \chi_0}, \tag{4.32}$$

with χ_0 the exact magnetic susceptibility we computed in section 4.2.1 (4.25). This last expression is the one Ding, B. *et al.* fitted to the experimental data [4]. The validity of this expression will be discussed in section 5.

4.3 Exact diagonnalization.

4.3.1 Size considerations.

As shown in section 4.1, the whole unit cell is very large. Each copper site carrying one spin. For the full unit cell, there are 96 of them. If we use the relation 4.10, we see that the biggest matrix would be of an order greater than 10^{96} which will be most likely forever out of the range of the computable. However, we can focus on a much smaller part of the unit cell for which one can perform computations. There is no obvious way to perform this reduction. But the range of possibilities is clearly restrained by our computational resources. In practice we were not able to perform computations for a greater number of sites than 15. The important features of the magnetic lattice are the trimers and the coordination number between the trimers, *i. e.* that a given trimer is coupled with six others.
But if one take simply seven trimers to represent the above fact, there is already 21 sites. For that number of sites, the biggest matrix size would be of 352'716x352'716 which could maybe be computed on some computers. Nonetheless, using periodic boundary conditions, it is possible to describe the interaction of a given with six others using 12 sites. This is shown on fig. 4.6.

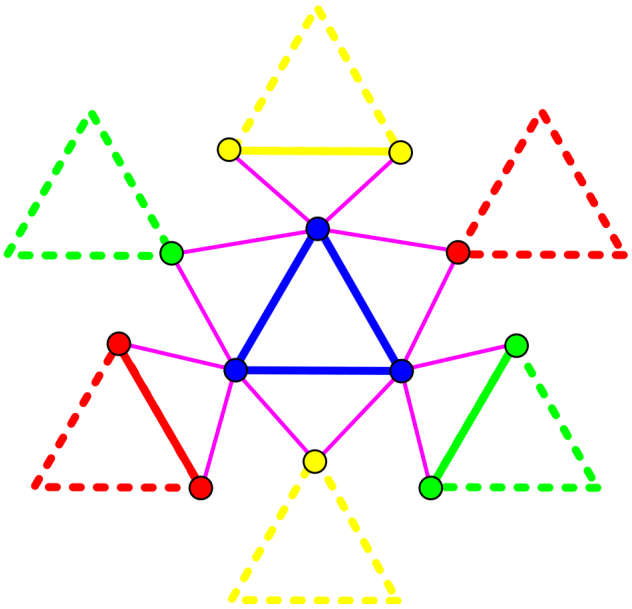

Figure 4.6: The reduced lattice used to model the interaction of a trimer with six others. The dotted lines represent the couplings through the periodic boundary. In that way, the sites of the same colour are coupled with the intra-trimer coupling through the periodic boundary.

One can expect very important size-effects for this model. Still it can bring qualitative information.

4.3.2 Algorithm

Generating the matrix corresponding to the Heisenberg Hamiltonian is fairly simple. The key point is that, without external field, this Hamiltonian contributes only on the bonds. To compute its matrix, one just need to iterate through each bond and compute its contribution.The process is the following:

- A table representing the bonds between the sites is inputted.
- The basis of the spin configuration is generated for each S_z^{total} sectors.

- A null matrix of the correct size is allocated.
- The process then iterate through each bound and compute its contribution. The $S_i^z S_j^z$ term brings a diagonal contribution and the $S_i^+ S_j^-$ and $S_i^- S_j^+$ terms bring two off-diagonal terms.

Once the matrix representation of the Hamiltonian is computed, we use an exact diagonnalization method from the fortran linear algebra package "LAPACK". Diagonnalization algorithms are a complex matter and we will not go through with a lot of details. The algorithm we used is based on the QR-algorithm. Using Householder transformations [6], one can transform a matrix A into a Hessenberg form. A Hessenberg matrix is a matrix which is almost triangular except the upper-diagonal terms. The Householder transformations are orthogonal, thus the new Hessenberg matrix has the same eigenvalues than the initial matrix. For a symmetric matrix, the Hessenberg form is also symmetric thus it is tri-diagonal. The QR-decomposition algorithm [7] is then used to get a triangular matrix. On a triangular matrix, the eigenvalues are listed on the diagonal so the problem is solved.Note that the QR-decomposition could be used without firstly using the Householder transformations but its computational cost is then greater. With these two steps, the overall complexity is $\mathcal{O}(n^3)$ where n is the matrix size.

4.3.3 Diagonnalization results.

The results of the exact diagonnalization are given in fig. 4.7 and fig. 4.8. We were not able to get a reasonable fit of these results with the experimental data. Nonetheless there are some common features. One can see that for small J_2 coupling, the susceptibility grows infinite at zero temperature, as it is expected for the isolated trimer ground state. On the other hand, when increasing the J_2 coupling, the system gain a singlet ground state with a null susceptibility as it is expected for an even number of interacting sites. But this last limit is not interesting for our case since our system behaves like weakly interacting trimers.
The most significant feature is clearly visible on the inverse susceptibility graph (fig. 4.8). For isolated trimers, the inverse susceptibility goes to zero at zero temperature. This is not anymore the case in the presence of a small inter-trimer coupling J_2. If one look at the second slope, it doesn't go to zero. The zero temperature susceptibility is therefore finite and its value depends on J_2. Nonetheless since we were not able to derive an analytical expression for this system, the exact dependence in J_2 could not be found.

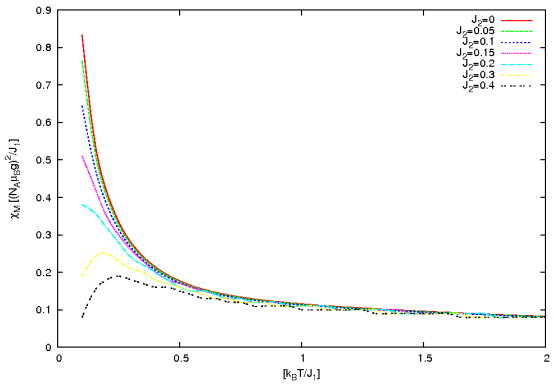

Figure 4.7: Magnetic susceptibility from the exact diagonnalization for different coupling ratios J_2/J_1.

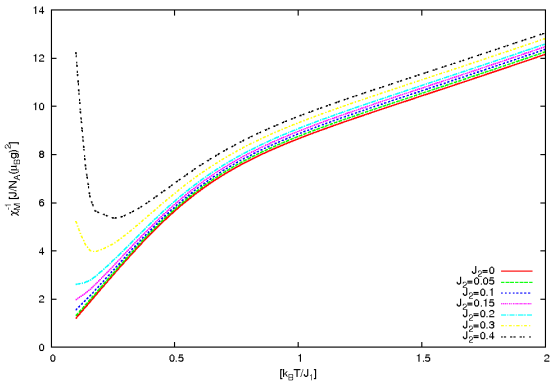

Figure 4.8: Inverse magnetic susceptibility from the exact diagonnalization for different coupling ratios J_2/J_1.

The size-effect on these computations remain very important. We performed some similar computations on different system size, going from 9 up to 15 sites. The results are shown in fig. 4.9. Seeing the massive

size effect, it is most likely that exact diagonnalization will not bring quantitative information about the system.

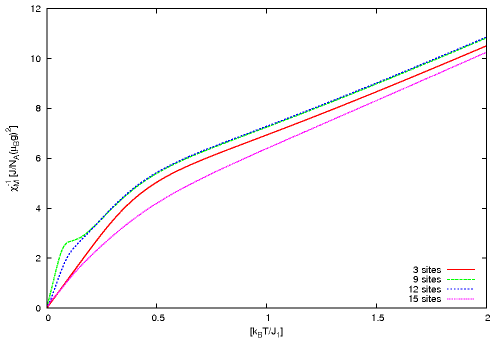

Figure 4.9: Magnetic susceptibility for 3, 9, 12 and 15 sites. These plots were obtained by adding interacting trimers to the single trimer. Thus it does not reproduce the correct coordination number for the number of interacting trimers. The differences between the plots could be called a size effect, but it also shows the importance of the trimer coordination number.

5 Fitting.

Even if the exact diagonnalization did not bring quantitative information we could fit with the experimental data, there are still some models we can use. The most basic one is the Curie-Weiss susceptibility:

$$\chi_M^{C-W} = \frac{C}{T-\theta} \tag{5.1}$$

Another model is the exact trimer susceptibility:

$$\chi_M = \frac{N_A(\mu_B g)^2}{k_B T} \frac{5exp\left(-\frac{3}{2}\left|J_1\right|\beta\right)+1}{4\left(exp\left(-\frac{3}{2}\left|J_1\right|\beta\right)+1\right)} \tag{5.2}$$

And finally, one can use the mean field susceptibility derived in section 4.2.2 (4.32):

$$\chi_M = \frac{(\chi_M)_{tri}}{1-\frac{2zJ_2}{N_A\mu_B^2 g^2}(\chi_M)_{tri}} \tag{5.3}$$

5.1 Curie-Weiss fits.

The inverse Curie-Weiss susceptibility is just a straight line those slope is $\frac{1}{C}$. It is thus very easy to fit it to the inverse susceptibility measurements. In the high temperature range, since we expect J_2 to be significantly smaller than J_1, the trimers should behave like they are essentially uncoupled. Linking the high temperature fit to the exact trimer susceptibility will give us a good approximation of the value of J_1. The fits are shown in fig. 5.1.

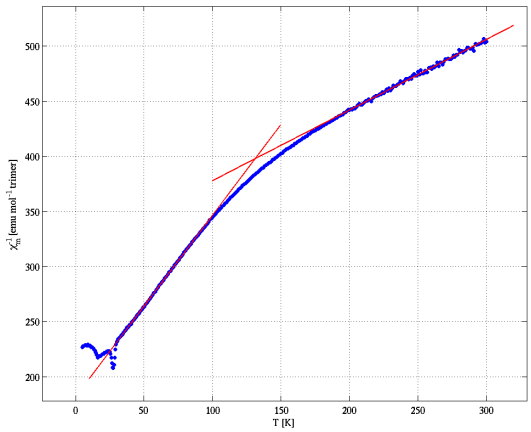

Figure 5.1: Inverse susceptibility measurements. The Currie-Weiss fits are performed in both slope regions.

The Curie-Weiss law is the same mean-field approximation we did in section 4.2.2. it is usually written in the form:

$$\chi = \frac{\chi 0}{1 - \frac{T_c}{T}}. \tag{5.4}$$

with the Curie susceptibility of a spin-$\frac{1}{2}$, the Curie-Weiss susceptibility can be written as:

$$\chi = \frac{C'}{T - T_c} \tag{5.5}$$

$$\text{where} \quad C' = \frac{N(g\mu_B)^2}{4Vk_B}. \tag{5.6}$$

The slopes on the fits are $\frac{1}{C'}$. We can now explain the second (sharpest) slope. In low temperatures, the trimers are in one of the four ground states which are of a total spin $\frac{1}{2}$. So they behave like spin-$\frac{1}{2}$'s. Therefore there are three times less sites in the system and then C' is three times smaller because of the sites density $\frac{N}{V}$. The second slope is therefore three times bigger than the first one, which we can verify on the fig. 5.1.
For the first slope, Taylor-expanding both Curie-Weiss and exact trimer susceptibility brings the dependency of the parameters C and θ in J_1 and g. we found:

$$g = \sqrt{\frac{4k_B C}{3N\beta^2}} \tag{5.7}$$

$$J_1 = 2k_B\theta \tag{5.8}$$

This brings the values of g and J_1 we found:

$$g = 2.356, \tag{5.9}$$

$$J = -115cm^{-1}. \tag{5.10}$$

5.2 Isolated trimer fits.

We stated above that the system is expected to behave like isolated trimers at high temperature. The point here is to determine where the insulated trimers picture breaks down. To investigate that, one fit the data

on the analytic expression for the trimer for different temperature ranges. Looking at the fitting parameters values we get, we might be able to see where the insulated trimers picture breaks down. This is done in fig. 5.2 for the value of J_1.

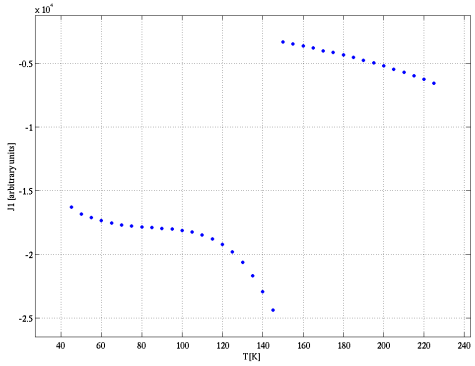

Figure 5.2: Variation of the fitted J_1 vs the lower boundary of the fitted temperature range.

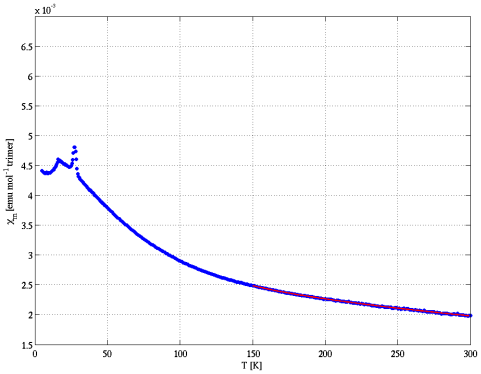

Figure 5.3: Best fit (red line) for the isolated trimer model on the appropriate temperature range. The obtained value of J_1 is -257.36 $[emu^{-1}moltrimer^{-1}]$.

We see a big discontinuity in the value of J_1 at approximately $150K$. If we look at the inverse susceptibility in fig. 5.1, we see that $150K$ is where the trimers are going to their ground state. This is the region where J_2 is important and therefore it is not surprising to see the insulated trimers picture breaking down at that point. The best fit in the appropriate temperature range is shown in fig. 5.3.

5.3 Mean field fits.

We apply the same method here than in section 5.2 but for the mean field expression we found in section 4.2.2. We will investigate the stability of both J_1 and J_2 with this model. The result is shown on fig. 5.4.

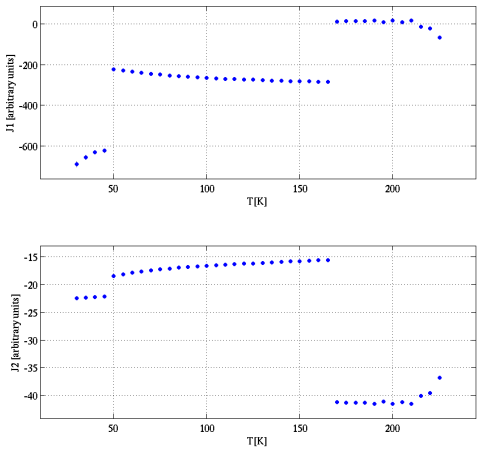

Figure 5.4: Variation of the fitted J_1 and J_2 vs the lower boundary of the fitted temperature range.

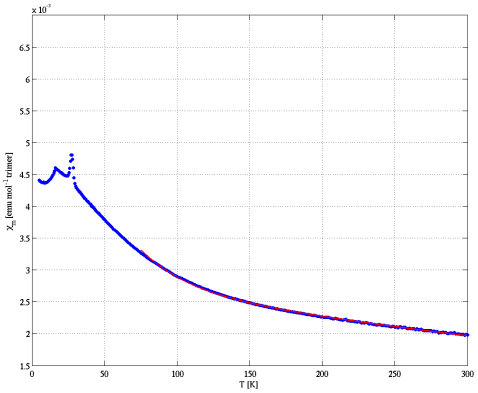

Figure 5.5: Best fit (red line) for the mean field model on the appropriate temperature range. The obtained values are -248.53 $[cm^{-1}]$ for J_1 and -17.24 $[cm^{-1}]$ for J_2.

The values of J_1 and J_2 are quite stable between $50K$ and $150 - K$. The mean field expression failing at low temperature is expected since its essential assumption is that the trimers are not correlated. This is indeed wrong at low temperatures where the J_2 coupling is of great importance.
But the mean field expression does also seem to fail at high temperatures. Again, looking at its expression (5.3), we find that it does not fullfill our initial intuition for high temperatures: For high temperatures we expect the system to behave like isolated trimers. So the dependency in J_2 should somehow vanish, which is not the case in expression (5.3). The best obtained fit is shown in fig. 5.5.

6 Conclusion.

Several approaches have been taken to model the metal-organic framework $\{[Cu_3(\mu_3{-}O)(\mu_3{-}trz)_3(OH)(H_2O)_6]\}_n$.
The analytic approach gives the exact trimer susceptibility and the weakly interacting trimer mean field susceptibility. Both models were found to be reasonable on the appropriate temperature range. While the exact trimer susceptibility was valid only at high temperatures above $150K$, the weakly interacting trimer mean field susceptibility was valid on a much smaller range, between $60K$ and $100 - 150K$.
This fact fullfill the intuition that the trimers must behave as essentially uncoupled at high temperatures, while the mean field approach fails at low temperatures where magnetic ordering is of great importance. Therefore there must be just a limited temperature range where the mean field approach is valid, which is what the fits seem to tell.
The numerical approach was attempted to model the inter-trimer couplings. Due to limitations in the system size, this last approach did not bring any usable quantitative data. Nonetheless the effect of the inter-trimer coupling could be observed, bringing the finite zero temperature susceptibility for the calculated curves, as it has been observed on the measurements.
Further work to characterise this system are for example the random phase approximation approach to derive an effective model instead of the Heisenberg Hamiltonian, or classical Monte Carlo simulations.

7 Acknowledgements

I would like to thank Henrik Ronnow and Gøran Nilsen for their support, as well as Andreas Läuchli for his help concerning the computational aspects of this project.

References

[1] David Sherrington and Scott Kirkpatrick. Solvable model of a spin-glass. *Phys. Rev. Lett.*, 35(26):1792–1796, Dec 1975.

[2] R. Moessner and J. T. Chalker. Properties of a classical spin liquid: The heisenberg pyrochlore antiferromagnet. *Phys. Rev. Lett.*, 80(13):2929–2932, Mar 1998.

[3] M. Matsuda, K. Kakurai, A. A. Belik, M. Azuma, M. Takano, and M. Fujita. Magnetic excitations from the linear heisenberg antiferromagnetic spin trimer system $a_3cu_3(po_4)_4$ (a = ca, sr, and pb). *Physical Review B (Condensed Matter and Materials Physics)*, 71(14):144411, 2005.

[4] B. Ding, L. Yi, P. Cheng, D.-Z. Liao, and S.-P. Yan. Synthesis and characterization of a 3d coordination polymer based on trinuclear triangular cu^{II} as secondary building units. *Inorganic Chemistry*, 45(15):5799–5803, 2006.

[5] B. D. Josephson. The discovery of tunnelling supercurrents. *Rev. Mod. Phys.*, 46(2):251–254, Apr 1974.

[6] Alston S. Householder. Unitary triangularization of a nonsymmetric matrix. *J. ACM*, 5(4):339–342, 1958.

[7] Gene H. Golub and Charles F. Van Loan. *Matrix computations*. Johns Hopkins University Press, Baltimore, MD, USA, 3 edition, 1996.

[8] Neil W. Ashcroft and David N. Mermin. *Solid State Physics*. Thomson Learning, Toronto, January 1976.